M. Chaieb

S. Tounsi

R. Neji

F. Sellami

J. Electrical Systems 4.1 (2008): 1-23

Regular paper

Design of a high-torque machine with two integrated motors axes reducing the electric vehicle consumption

The motorization of electric vehicle needs to work at a constant power on a wide range of speed. In order to be able to satisfy these requirements, we describe in this paper a solution, which consists in modifying of a simple structure of a permanent magnet motor by a double rotor structure integrating two motor axes into the same machine. This article describes, then, a design methodology of a permanent magnet motor with double rotor, radial flux, and strong starting torque for electric vehicles. This work consists on the analytical dimensioning of the motor by taking into account several operation constraints followed by a modelling by the finite elements method. This study is followed by the comparison between this motor and a motor with one rotor. A global model of the motor- converter is developed for the purpose to answer several optimisation problems.

Keywords: Electric vehicle, Dimensioning, Permanent magnet motor, Finite elements, Double rotor

1. INTRODUCTION

The electric vehicle becomes a topical research theme; the manufacturers of vehicles, batteries, and electric motors, now group gather their efforts of research to answer the specifications prepared by the different environment services.
The electric solution satisfies the requirements of urban traffic; absence of gas and noise pollution.
The application of electric vehicle requires the use of motors with important starting torque.
The choice of a double rotor structure to get an important torque which is the sum of the two torque delivered by the two rotors [1].
This structure is presented and studied by the analytical method. This method is based on the fundamental electromagnetism law. The dimensioning solution obtained is validated by simulations with using of the finite elements method.
The dimensioning of a motor poses an optimization problem, which consists in finding of the optimum parameters of conception for maximum motor-converter efficiency by using the genetic algorithms method [2].

2. THE ELECTRIC VEHICLE STARTING TORQUE

According to the diagram of NREITS (National Research Institute of Transport and its security) the electric vehicle wheels speed starts from a null speed until it reaches its basic speed. During this phase the motor exerts a constant starting torque on the wheels. Thin, from a null speed until the maximum vehicle speed the motor exerts a torque, which decreases in proportion to the speed (area of constant power) [3].

Laboratoire d'Electronique et des Technologies de l'Information -LETI- , Ecole Nationale d'Ingénieurs de Sfax
B.P. W, 3038 Sfax – Tunisie. E-mail: Chaieb_med@yahoo.fr, souhir.tounsi@enis.rnu.tn,, rafik.neji@enis.rnu.tn, faycal@sellami.com

The figure 1 presents the torque in function of the wheels speed.

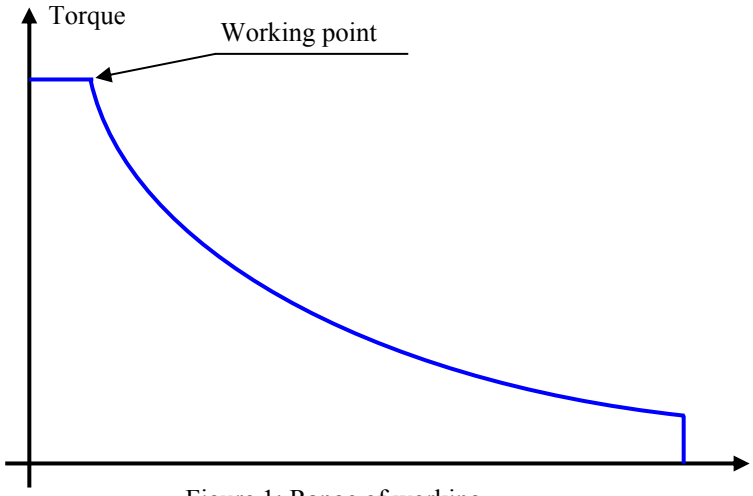

Figure 1: Range of working

The point indicated on the previous figure 1 is the basic operation point characterized by its basic speed (V_b) and by its torque equals to the starting torque (T_d).
The total torque, which must be delivered by the driving wheels, is given by the following expression that is inspired from the fundamental dynamics law describing the movement of the vehicle [4]:

$$T_w = T_{rt+} T_a + T_c + \sigma M (R_w)^2 dV/dt \quad (1)$$

With, T_{rt} is the friction rolling resistance.

$$T_{rt} = R_w f_r Mg \quad (2)$$

f_r is the coefficient of the tire rolling resistance that depends on the wheels width and on the road coating.
T_a is the aerodynamic torque.

$$T_a = R_{w(} M_{va} C_x A_f) / 2V^2 \quad (3)$$

This torque is then proportional to the air density (M_{va}=1.28kg/m^3), to aerodynamic drag coefficient (C_X = 0.7), to the square of the speed and the frontal area of the vehicle (A_f =1.4 m^2).
T_c is the climbing resistance.

$$T_c = R_w Mg \sin(\lambda) \quad (4)$$

Where,

- λ : angle that makes the road with the horizontal.
- R_w: wheel radius.
- M: vehicle mass.
- σ: coefficient taking into account the inertia of turning elements (wheels, motor tree, transmission of power).
- V: vehicle speed.

In this condition and by neglecting the friction rolling resistance force and the aerodynamic force, the torque at beginning becomes:

$$T_d = M R_w \left(\frac{R_w \sigma V_b}{t_d} + g \sin(\lambda) \right) \quad (5)$$

td is the starting time.

3. ANALYTICAL DIMENSIONING OF THE MOTOR

3.1. CONFIGURATION

The motor with double rotor is made up of two stators and two rotors. Each stator contains four pole pairs and six main teeth. Between two main teeth an inserted tooth is added to improve the waveform and reduce the flux leakages. Each phase winding is made up of four coils diametrically opposed.
The configuration of the motor is characterized by a relationship between the number of teeth and the number of pole pairs directly bound to the space percentage occupied by the slots compared to that occupied by the inserted tooth [5].
The figure 2 represents a permanent magnet motor with double rotor.

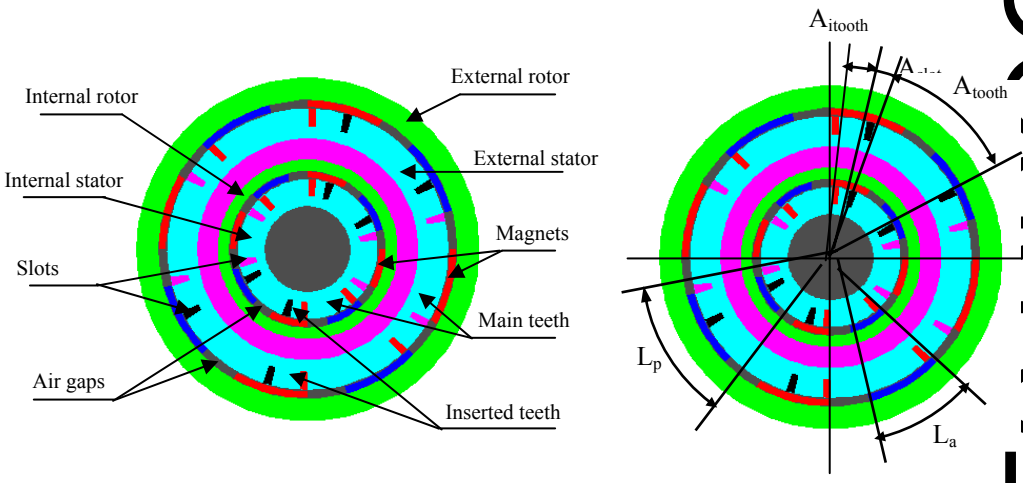

Figure 2: Configuration of a permanent magnets motor with double rotor

3.2. STRUCTURE

The design and form of the machine are defined by basing on the three following ratios:
The first coefficient is the ratio β of the magnet angular width L_a by the pole pitch L_p

$$\beta = \frac{L_a}{L_p}, \text{ with } L_p = \frac{\pi}{P} \quad (6)$$

Where P is the pairs pole number.
The second coefficient is the ratio α of the main tooth angular width A_{tooth} by the magnet angular width:

$$\alpha = \frac{A_{tooth}}{L_{aam}} \quad (7)$$

It adjusts the size of the main tooth and has a strong influence on the electromotive force.

The last coefficient is the ratio of the inserted tooth A_{itooth} by a main tooth A_{tooth} it fixes the inserted tooth size

$$R_{it} = \frac{A_{itooth}}{A_{tooth}} \tag{8}$$

The size of the inserted tooth is optimised by the finite elements method in order to reduce flux leakages and ripple torque [6].
The advantage of these coefficients is to quickly define the form of the machine.
The electromotive force will be expressed in function to these ratios [7].

3.3. Geometric size of the motor

The figure 3 shows the width of the interior slot L_{slot1} and the width of the exterior slot L_{slot2} with R_{m1} and R_{m2} are the radius of the interior and exterior stators.

L_{slot1} and L_{slot2} represent the slots angular width, which are expressed as follows.

$$L_{slot\,1} = \frac{D_{m1} - e_1 - H_{d1}}{2} A_{slot} \tag{9}$$

$$L_{slot\,2} = \frac{D_{m2} - e_2 - H_{d2}}{2} A_{slot} \tag{10}$$

Where:

- D_{m1} and D_{m2}: stators diameter
- e_1 and e_2: air-gaps thickness
- H_{d1} and H_{d2}: teeth height
- A_{slot}: slot angular width

The teeth height allow keeping necessary space for the copper, it has therefore a relationship with the total number of conductors occupied by slots and the current density.

$$H_{d1} = \frac{N_{sph\,1} I_{ph}}{2 N_d \delta K_r L_{slot\,1}} \tag{11}$$

$$H_{d2} = \frac{N_{sph\,2} I_{ph}}{2 N_d \delta K_r L_{slot\,2}} \tag{12}$$

Where:

- N_d: main teeth number
- N_{sph}: number of spire per phase
- I_{ph}: phase current
- δ : current density in coils
- K_r: filling coefficient of slot

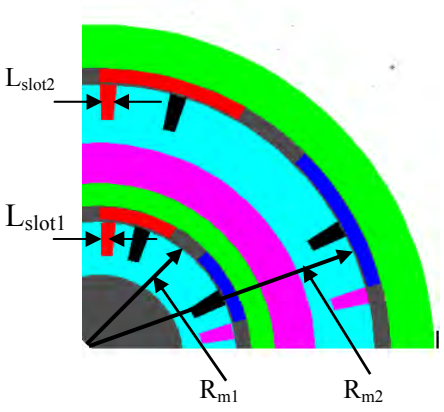

Figure 3: Average width of slots

Replacing L_{slot} by its expression:

$$H_{d1} = \sqrt{\frac{N_{sph1} I_{ph}}{\sqrt{2} N_d \delta K_r A_{slot}} + \left(\frac{D_{m1} - e_1}{2}\right)^2} - \frac{D_{m1} - e_1}{2} \tag{13}$$

$$H_{d2} = \sqrt{\frac{N_{sph\,2} I_{ph}}{\sqrt{2} N_d \delta K_r A_{slot}} + \left(\frac{D_{m2}\text{-}e_2}{2}\right)^2} - \frac{D_{m2}\text{-}e_2}{2} \tag{14}$$

The section of the main tooth related to the interior stator is given by the following expression:

$$S_{d1} = \frac{D_{m1}\text{-}e_1}{2} A_{tooth} L_m \tag{15}$$

With L_m is the motor length.
The section of the main tooth related to the exterior stator is given by the following expression:

$$S_{d2} = \frac{D_{m2}\text{-}e_2}{2} A_{tooth} L_m \tag{16}$$

The section of the inserted tooth related to the interior and exterior stator is given by:

$$S_{di1} = \frac{D_{m1}\text{-}e_1}{2} A_{itooth} L_m \tag{17}$$

$$S_{di2} = \frac{D_{m2}\text{-}e_2}{2} A_{itooth} L_m \tag{18}$$

The Section of the slot related to the interior stator is expressed as follows

$$S_{e1} = A_{slot}.\frac{D_{m1} - e_1}{2} L_m = \frac{1}{2}\left[\frac{2\pi}{N_d} - A_{tooth} - A_{itooth}\right]\frac{D_{m1} - e_1}{2} L_m \tag{19}$$

The Section of the slot related to the exterior stator:

$$S_{e2} = A_{slot}.\frac{D_{m2} - e_2}{2} L_m = \frac{1}{2}\left[\frac{2\pi}{N_d} - A_{tooth} - A_{itooth}\right]\frac{D_{m2} - e_2}{2} L_m \tag{20}$$

The thickness of the stator yoke H_{cs} is determined by the flux conservation theorem between a half of the main tooth and the yoke.

$$\frac{\Phi}{2} = \frac{B_d\ S_d}{2} = H_{cs}\ B_{cs}\ L_m \Leftrightarrow H_{cs1} = \frac{B_{d1}\ S_{d1}}{2\ L_m\ B_{cs1}} \tag{21}$$

$$H_{cs2} = \frac{B_{d2}\ S_{d2}}{2\ L_m\ B_{cs2}} \tag{22}$$

Where:

- B_d: flux density in the teeth
- B_{cs}: flux density in the stator yoke

The magnet height fixes the flux density in the air-gap. This parameter is given by applying the ampere law for a maximal covering a magnet and a main tooth. The flux created by magnets is composed of the leakage flux between magnets and the flux in stator and rotor H_{a1} and H_{a2} represent the magnet height of the interior and external rotor

$$H_{a1} = \frac{\mu_a\ B_{e1}\ e_1}{B_r - \frac{B_{e1}}{K_{fu}}} \tag{23}$$

$$H_{a2} = \frac{\mu_a \; B_{e2} \; e_2}{B_r - \frac{B_{e2}}{K_{fu}}} \tag{24}$$

With,

- μ_a : magnet relative permeability
- B_r: magnet remanence.
- K_{fu}: coefficient of flux leakages
- B_e: air-gap flux density

Exactly like with the determination principle of the yoke stator thickness, the yoke rotor thickness H_{cr} is determined by the application of flux conservation theorem between half of a magnet and the yoke.

$$\frac{\Phi}{2} = B_{cr} \; H_{cr} \; L_m \; K_{fu} = \frac{B_e \; S_d}{2} \quad \Leftrightarrow \quad H_{cr1} = \frac{B_{e1} \; S_{d1}}{2 \; K_{fu} \; L_m \; B_{cr1}} \tag{25}$$

$$\Leftrightarrow H_{cr\,2} = \frac{B_{e\,2} \; S_{d\,2}}{2 \; K_{fu} \; L_m \; B_{cr\,2}} \tag{26}$$

Where, B_{cr} is the flux density in the rotor yoke.

3.4. ANALYTICAL ESTIMATION OF THE ELECTROMOTIVE FORCE RELATED TO ONE STATOR AND ONE ROTOR

The electromotive force deduced from the flux derivative, we need therefore to know the flux in versus magnets position. [8, 9]

The flux leakage between the air-gap and the stator is neglected and the magnetic induction is supposed to be perfectly rectangular in the air-gap. [10, 11]

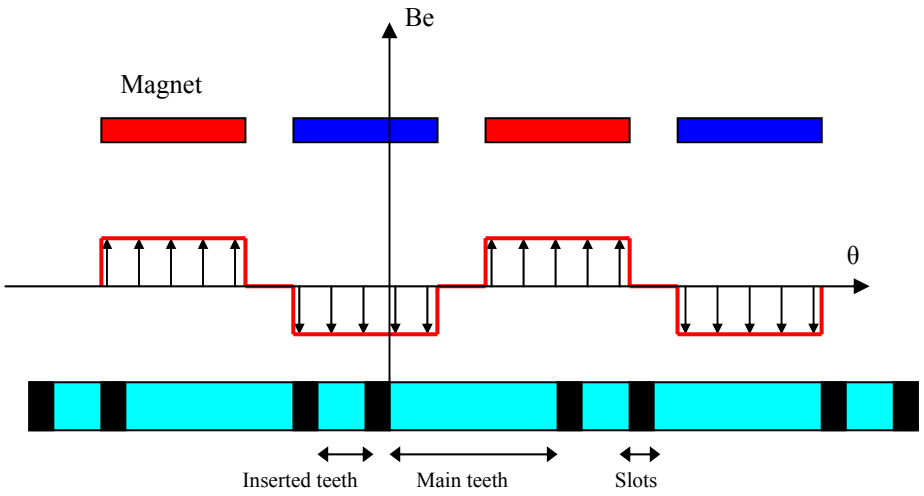

Figure 4: Flux density in the air-gap

For a stator, the flux in a coil can be put in the following form:

$$\varphi_b = \int_{S_{coil}} Be\,(\theta e\,(\theta = \int_{\theta-\frac{A_{tooth}}{2}}^{\theta+\frac{A_{tooth}}{2}} Be(\theta e(\theta) \tag{27}$$

The figure 4 shows the initial position from which the rotor moves with angular velocity (Ω).

Four distinct intervals, according to magnets position and geometrical parameters values, which gives.

$$\begin{aligned}
&-\frac{|L_a - A_{tooth}|}{2} \le \theta \le \frac{|L_a - A_{tooth}|}{2} \Rightarrow \quad \varphi_b = \frac{L_m.D_m}{2}.A_{tooth}.B_e \\
&\frac{L_a - A_{tooth}}{2} \le \theta \le L_p - \frac{L_a + A_{tooth}}{2} \Rightarrow \quad \varphi_b = \frac{L_m D_m}{2}\left(\frac{L_a + A_{tooth}}{2} - \theta\right) B_e \\
&L_p - \frac{L_a + A_{tooth}}{2} \le \theta \le \frac{L_a + A_{tooth}}{2} \Rightarrow \quad \varphi_b = \frac{L_m.D_m}{2}(L_p - 2.\theta).Be \\
&\frac{L_a + A_{tooth}}{2} \le \theta \le L_p - \frac{L_a - A_{tooth}}{2} \Rightarrow \quad \varphi_b = \frac{L_m D_m}{2}\left(L_p - \left[\frac{L_a + A_{tooth}}{2}\right] - \theta\right) B_e
\end{aligned} \tag{28}$$

The electromotive force at no-load is: $E = -\Omega N_{sph} \frac{d\varphi}{d\theta}$ (29)

By intervals, the electromotive force of a phase is given by the following equations:

$$\begin{aligned}
&-\frac{|L_a - A_{tooth}|}{2} \le \theta \le \frac{|L_a - A_{tooth}|}{2} \Rightarrow E = 0 \\
&\frac{L_a - A_{tooth}}{2} \le \theta \le L_p - \frac{L_a + A_{tooth}}{2} \Rightarrow E = N_{sph}\,\Omega \frac{L_m D_m}{2} B_e \\
&L_p - \frac{L_a + A_{tooth}}{2} \le \theta \le \frac{L_a + A_{tooth}}{2} \Rightarrow E = 2N_{sph}\Omega \frac{L_m D_m}{2} B_e \\
&\frac{L_a + A_{dent}}{2} \le \theta \le L_p - \frac{L_a - A_{dent}}{2} \Rightarrow E = N_{sph}\Omega \frac{L_m D_m}{2} B_e
\end{aligned} \tag{30}$$

Where, Ω is the angular speed.

The emf evolution over an electric period is odd periodic function of the period T, it may resemble a sinus function. The electromotive force may take the following form:

$$emf = \sum_{1}^{n} b_n.\sin\left(\frac{2\pi}{T}\theta\right) \tag{31}$$

$$\text{With } b_n = \frac{4}{T}\int_{\theta_0}^{\theta_0+T/2} E(\theta)\sin\left(\frac{2\pi}{T}\theta\right)d\theta \text{ and } \theta = -\frac{|L_a - A_{tooth}|}{2} \tag{32}$$

This gives the first harmonic of the electromotive force in a stator:

$$emf(t) = \frac{8}{\pi} N_{sph}\, L_m\, D_m\, B_e \sin\left(\frac{\pi}{2}\beta\right)\sin\left(\frac{\pi}{2}\beta\,\alpha\right)\Omega\ \sin(p\,\Omega\,t) \tag{33}$$

Thus, the total electromotive force of the motor is:

$$emf(t)=\frac{8}{\pi} N_{sph1}\, L_m\, D_{m1}\, Be_1\, \sin\left(\frac{\pi}{2}\,\beta\right)\, \sin\left(\frac{\pi}{2}\,\beta\beta\right)\, \Omega_m \sin(p\,\Omega_m\, t)+ \frac{8}{\pi} N_{sph2}\, L_m\, D_{m2}\, Be_2\, \sin\left(\frac{\pi}{2}\,\beta\right)\, \sin\left(\frac{\pi}{2}\,\beta\beta\right)\, \Omega_m \sin(p\,\Omega_m\, t) \quad (34)$$

We deduce then the electric constant of the motor:

$$Ke=\frac{12}{\pi} N_{sph1}\, L_m\, D_{m1}\, Be_1 \sin\left(\frac{\pi}{2}\,\beta\right)\sin\left(\frac{\pi}{2}\,\beta\,\alpha\right)+\frac{12}{\pi} N_{sph2}\, L_m\, D_{m2}\, Be_2 \sin\left(\frac{\pi}{2}\,\beta\right)\sin\left(\frac{\pi}{2}\,\beta\,\alpha\right) \quad (35)$$

3.5. MAXIMAL CURRENT OF DEMAGNETIZATION

To avoid demagnetization, the phase current must be inferior to the maximal current of the demagnetization of interior I_{max1} and exterior I_{max2} stators magnets.

$$I_{max1} = \frac{p}{3\mu_0 N_{sph1}}\left[\left(B_r[1+\alpha_m(t_a-20)]-B_c\right)H_{a1}-\frac{B_c K_{fu} e_1}{\mu_a}\right] \quad (36)$$

$$I_{max2} = \frac{p}{3\mu_0 N_{sph2}}\left[\left(B_r[1+\alpha_m(t_a-20)]-B_c\right).H_{a2}-\frac{B_c K_{fu} e_2}{\mu_a}\right] \quad (37)$$

Where:

- μ_0 : air permeability
- t_a: magnet temperature
- B_c: minimum flux density allowed in the magnets

3.6. A PHASE RESISTANCE

The spire average length L_{sp} for a stator is given by the following expression:

$$L_{sp} = 8L_m\, A_{slot}\left(\frac{D_m - e - H_d}{2}\right) \quad (38)$$

Then, we may get an expression of a motor phase resistance.

$$R_{ph} = R_{cu}(Tb)\frac{N_{sph1}\,\delta\, L_{sp1}}{I_{ph}} + R_{cu}(T_b)\frac{N_{sph2}\,\delta\, L_{sp2}}{I_{ph}} \quad (39)$$

With, R_{cu} (T_b): copper resistivity to the coil temperature T_b lark.

3.7. MAGNETIC REACTION OF AN ARMATURE

We look for an estimation of the flux variation at load compared to the flux variation at no-load. Indeed, in nominal operation, the armature is crossed by a current and creates through the coil a flux reaction. This flux is opposed to the flux produced by the magnets, which deforms and reduce the electromotive force. For this estimation we consider that iron has an infinite permeance and that the magnet permeability is equal to the one of the air.

The application of the Ampere law gives:

$$2\left(H_e e + H_e H_a\right) = \frac{N_{tc} I_{ph}}{N_d} \Leftrightarrow \frac{B_{ri}\left(e + H_a\right)}{\mu_0} = \frac{N_{tc} I_{ph}}{N_d}$$

Then:

$$B_{ri1} = \frac{\mu_0 N_{tc} I_{ph}}{N_d\left(e_1 + H_{a1}\right)} \tag{40}$$

$$B_{ri2} = \frac{\mu_0 N_{tc} I_{ph}}{N_d\left(e_2 + H_{a2}\right)} \tag{41}$$

Where

- B_{ri}: armature reaction flux density
- N_{tc}: total number of conductor

3.8. NUMBER OF SPIRE PER PHASE

The motor is characterized by number of slot total conductors N_{tc} given by the following expression:

$$N_{tc} = \frac{3K_e L_{sp}}{2B_e S_a} \tag{42}$$

Each spire is composed by two conductors, this allows us enables us to deduce the formula of spire number per phase for a three-phase machine:

$$N_{sph} = \frac{K_e L_{sp}}{4B_e S_a} \tag{43}$$

Where S_a is the magnet section.

3.9. MOTOR DIAMETER

The exterior diameter of motor is given by the following formula:

$$D_m = D_{m1} + e_1 + 2\left(H_{cr1} + H_{a1} + H_{cs2} + H_{d2} + e_{rs} + e_2 + H_{a2} + H_{cr2}\right) \tag{44}$$

Where e_{rs} is the vacuum between rotor one and stator two.

3.10. SPECIFIC POWER OF A MOTOR

The specific power of the motor P_s (W/kg) is defined by the ratio of the electric power to the total mass:

$$P_s = \frac{P_{em}}{M_{tot}} \tag{45}$$

The total mass of the motor M_{tot} is the sum of masses of the stator teeth M_{ds}, the inserted teeth M_{di}, the stator yoke M_{cs}, the copper M_{cu}, the magnets M_{ai} and the rotor yoke M_{cr}.

$$M_{tot} = M_{ds1} + M_{di1} + M_{ai1} + M_{cs1} + M_{cr1} + M_{cu1} + M_{ds2} + M_{di2} + M_{ai2} + M_{cs2} + M_{cr2} + M_{cu2} \tag{46}$$

M_{ds1} and M_{ds2} represent respectively the mass of teeth of the interior and exterior stator.

$$M_{ds1} = \frac{A_{tooth} N_d}{2}\left[\left(\frac{D_{m1} - e_1}{2}\right)^2 - \left(\frac{D_{m1} - e_1}{2} - H_{d1}\right)^2\right] L_m M_{vt} \tag{47}$$

$$M_{ds2} = \frac{A_{tooth}\ N_d}{2}\left[\left(\frac{D_{m2} - e_2}{2}\right)^2 - \left(\frac{D_{m2} - e_2}{2} - H_{d2}\right)^2\right] L_m\ M_{vt} \tag{48}$$

Where, M_{vt} is the density of metal sheets.
M_{cs1} and M_{cs2} represent respectively the mass of the yoke of the interior and exterior stator.

$$M_{cs1} = \pi\left[\left(\frac{D_{m1} - e_1}{2} - H_{d1}\right)^2 - \left(\frac{D_{m1} - e_1}{2} - H_{d1} - H_{cs1}\right)^2\right] L_m M_{vt} \tag{49}$$

$$M_{cs2} = \pi\left[\left(\frac{D_{m2} - e_2}{2} - H_{d2}\right)^2 - \left(\frac{D_{m2} - e_2}{2} - H_{d2} - H_{cs2}\right)^2\right] L_m M_{vt} \tag{50}$$

M_{cu1} and M_{cu2} represent the mass of copper.

$$M_{cu1} = \frac{3\ I_{ph}\ N_{sph1}\ L_{sp}}{\sqrt{2}\ \delta}\ M_{vc} \tag{51}$$

$$M_{cu2} = \frac{3\ I_{ph}\ N_{sph2}\ L_{sp}}{\sqrt{2}\ \delta}\ M_{vc} \tag{52}$$

Where, M_{vc} is the copper density.
M_{ai1} and M_{ai2} represent the mass of the interior and exterior magnets.

$$M_{ai1} = p\ L_m L_a\left[\left(\frac{D_{m1} + e_1}{2} + H_{a1}\right)^2 - \left(\frac{D_{m1} + e_1}{2}\right)^2\right] M_{va} \tag{53}$$

$$M_{ai2} = p\ L_m L_a\left[\left(\frac{D_{m2} + e_2}{2} + H_{a2}\right)^2 - \left(\frac{D_{m2} + e_2}{2}\right)^2\right] M_{va} \tag{54}$$

With, M_{va} is the magnet density.
M_{cr1} and M_{cr2} represent the mass of the yoke of the interior and exterior rotor.

$$M_{cr1} = \pi\left[\left(\frac{D_{m1} + e_1}{2} + H_{a1} + H_{cr1}\right)^2 - \left(\frac{D_{m1} + e_1}{2} + H_{a1}\right)^2\right] L_m\ M_{vt} \tag{55}$$

$$M_{cr2} = \pi\left[\left(\frac{D_{m2} + e_2}{2} + H_{a2} + H_{cr2}\right)^2 - \left(\frac{D_{m2} + e_2}{2} + H_{a2}\right)^2\right] L_m\ M_{vt} \tag{56}$$

M_{di1} and M_{di2} represent the mass of the Inserted teeth of the interior and exterior stator.

$$M_{di1} = \frac{M_{d1}\ A_{itooth}}{A_{tooth}} \tag{57}$$

$$M_{di2} = \frac{M_{ds}\ A_{itooth}}{A_{tooth}} \tag{58}$$

3.11. THE MACHINE PARAMETERS

After the implementation of the design procedure, the following machine parameters are achieved, which is summarized in table 1.
The machine is a radial-flux permanent-magnet motor with double rotor configuration. The nominal power of the machine is 23 kW and its nominal rotational speed is 2500 min^{-1}.

Table 1: The main parameters of the machine

Parameter	Value
Rated electric power	23 kW
Rated speed	2500 min^{-1}
Electromagnetic torque	95 Nm
Electromotive force of the motor	472 V
Electric constant of the motor	2,32
Phase current	28 A
Number of pole pairs	4
Stator slots number per stator	12
Main teeth number per stator	12
Permanent magnets remanence flux density	1,17 T
Number of spire per phase	120
Air-gaps thickness	1 mm
Air-gap flux density	0,89 T
Permanent magnet height	5 mm
Interior stator teeth height	11 mm
Exterior stator teeth height	6 mm
Motor length	0,25 m
Motor diameter	0,24 m
Permanent magnet mass	4,2 kg
Motor mass	68 kg
Specific power of a motor	0,33 kW/kg
Efficiency	95%

4. FINITE ELEMENTS MODELLING OF THE ELECTRIC MOTOR

The modelling by finite elements is a study of complementarities and the validation of equations of the analytical dimensioning [12].
A parameterized model including many parameters is developed. The increase of the number of nodes is necessary to have a good temporal representation. The finite elements problem is resolved by the use of Maxwell-2D, a software package for analyzing electromagnetic fields in cross-sections of structures. Maxwell-2D uses finite elements analysis to solve two-dimensional (2D) electromagnetic problems [13].

4.1. FINITE ELEMENTS STUDY OF THE MOTOR

The study of the performances of the studied machine is carried out from two simulations, which characterize the machine. The first consists in carrying out a simulation at no-load to analyse the form and amplitude of the emf. The second is carrying out a simulation at load.

4.2. MOTOR STUDY AT NO LOAD

The studied machine is driven into rotation at its nominal speed at no-load. In these conditions, the simple tension corresponds to the emf.
The representation of the fields lines, obtained from a simulation is represented on the figure 5.

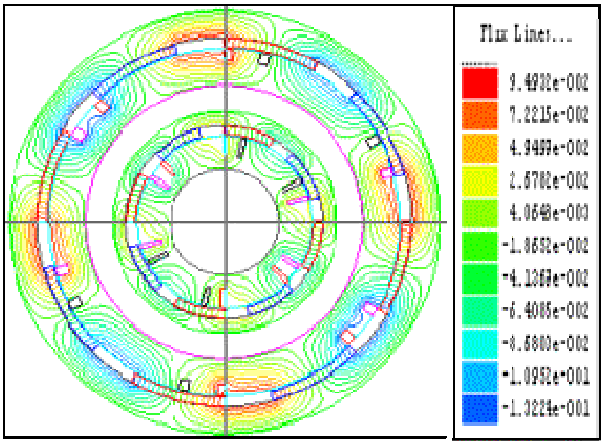

Figure 5: Lines of fields for an initial position

For different positions of the rotor, the winding captured flux of the machine is represented on the figures 6 and 7.

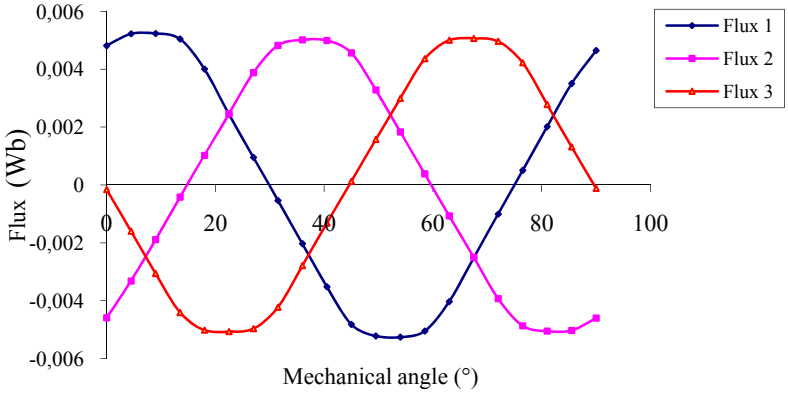

Figure 6: Flux through the three phases of the interior stator

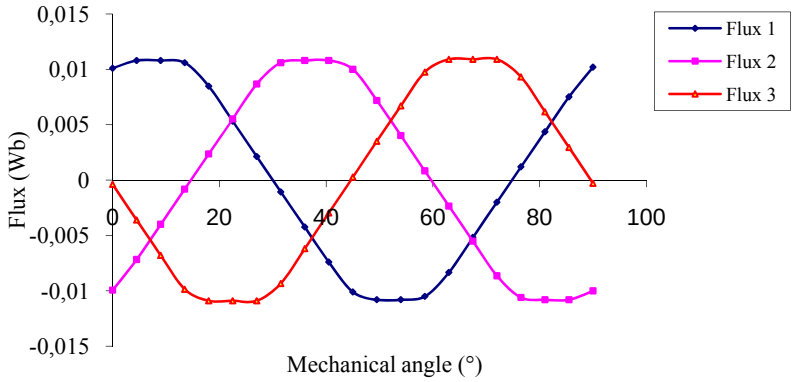

Figure 7: Flux through three phases of the exterior stator

The electromotive forces at no-load of the three phases for the two stators are represented on the figures 8 and 9.

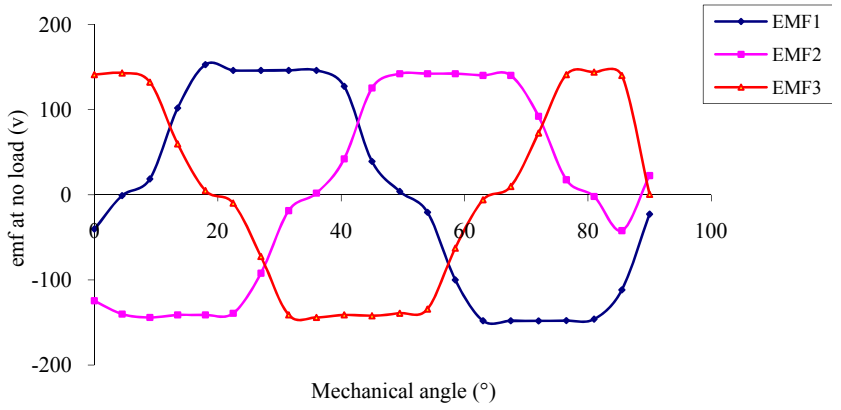

Figure 8: Electromotive forces at no load of the interior stator

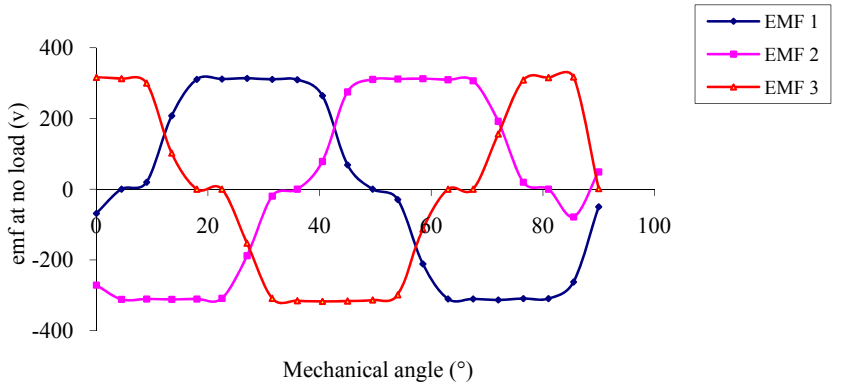

Figure 9: Electromotive forces at no load of the exterior stator

The form of the emf is trapezoidal. The light deformation at the bearing level is due to leakage flux variable in function to the angular position of the rotor.

4.3. STUDY OF THE MOTOR AT LOAD

The figures 10 and 11 represent the forms of the electromotive forces at the three phases levels after the feeding of the motor with a three-phase current system.

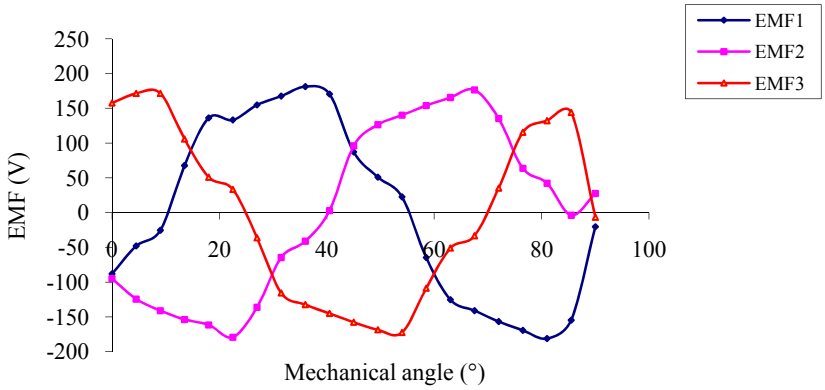

Figure 10: Electromotive forces at load of the interior stator

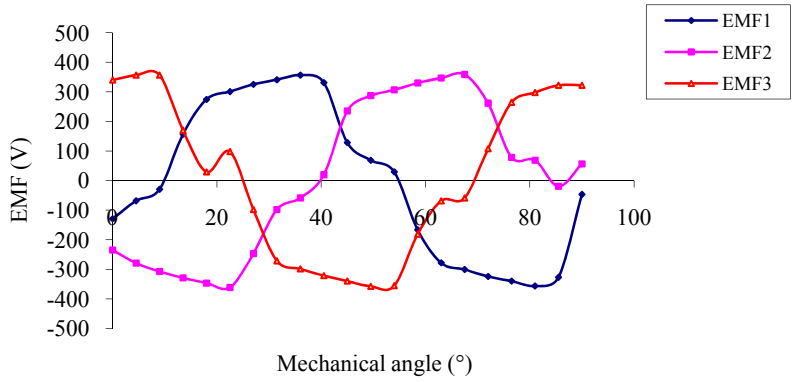

Figure 11: Electromotive forces at load of the exterior stator

The emf at load is just like the emf at no-load because the magnetic reaction of the armature is weak.

We suppose that the electromotive force at no-load is equal to the electromotive force at load (armature reaction is neglected) the electromagnetic torque of the motor is given in the following expression.

$$T_{em}(\theta) = \frac{1}{\Omega}\sum_{i=1}^{3} E_{1i}(\theta) I_{phi}(\theta) + \frac{1}{\Omega}\sum_{i=1}^{3} E_{2i}(\theta) I_{phi}(\theta) \qquad (59)$$

Where, E_i and I_{phi} are respectively the electromotive force and the phase current.

The electromagnetic torques produced by the two rotors of the synchronous machine is represented in the following figures:

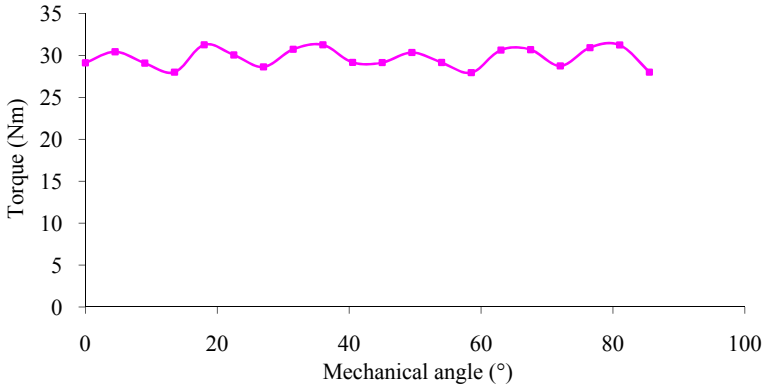

Figure 12: Electromagnetic torques of the interior rotor

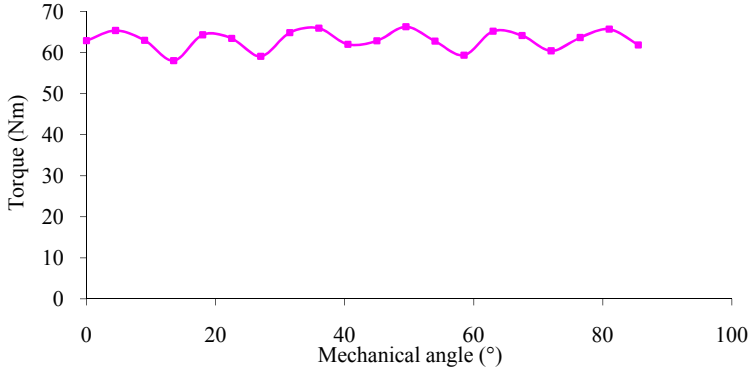

Figure 13: Electromagnetic torques of the exterior rotor

The total torque of the motor is the sum of the two torques produced by the two rotors, is represented on the figures 14.

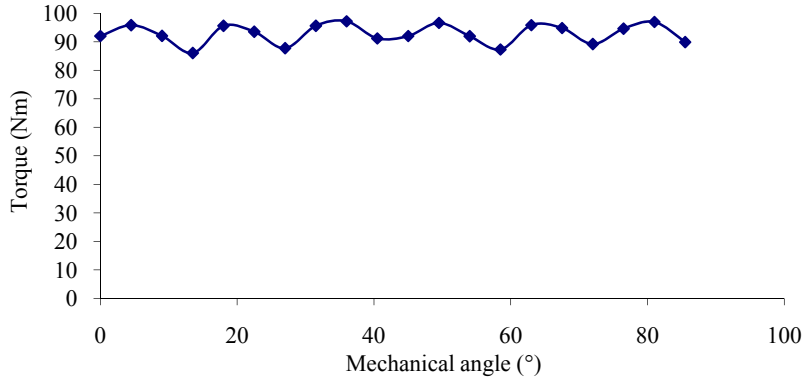

Figure 14: Electromagnetic torque of the motor

Table 2: Comparison between analytical and FE-methods

Parameter	analytical computation	finite elements method
Interior stator flux amplitude	0,0058 Wb	0,0052 Wb
Exterior stator flux amplitude	0,017 Wb	0,011 Wb
Interior stator EMF amplitude	155 V	150 V
Exterior stator EMF amplitude	317 V	310 V
Average electromagnetic torque	95 Nm	92 Nm

Table 2 shows a comparison between the values derived from the analytical computation and from the finite elements method. The analytical computation is more general, this means no assumptions are made about the iron nonlinearity, iron losses or current induced by spatial harmonics in the machine's conducting regions.
The values computed with the analytical computation and those computed with the finite elements method are coherent. Finally, the finite elements approach validates the analytical computation. The torque value given for the sizing is effectively achieved.

5. Study of the Motor Performances

Let's compare results obtained with the dimensioning of simple rotor motor for the same application and in identical conditions of use. The dimensioning procedure of these machines uses the same way of calculations that used for the double rotor electric motor. [14]
The figures 15 and 16 represent respectively the variation of the mass and specific power in function to the power of a motor with double rotor and a motor with one rotor.
This figure shows the benefit of using a motor with double rotor for the electric traction field, which necessitates a strong power.

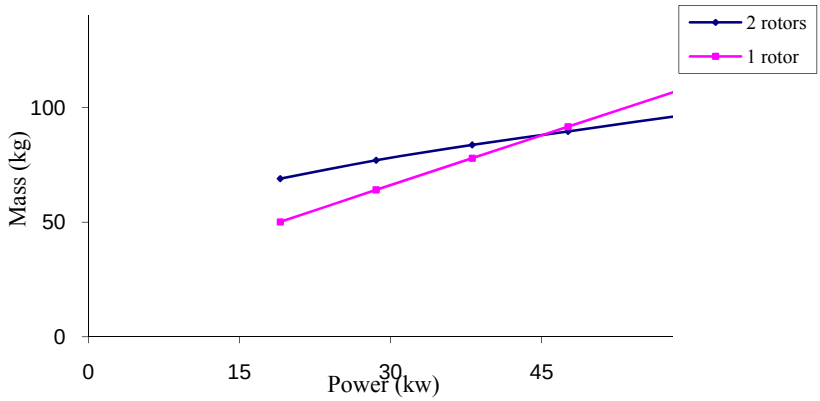

Figure 15: Mass of a motor with one rotor and of a motor with double rotor

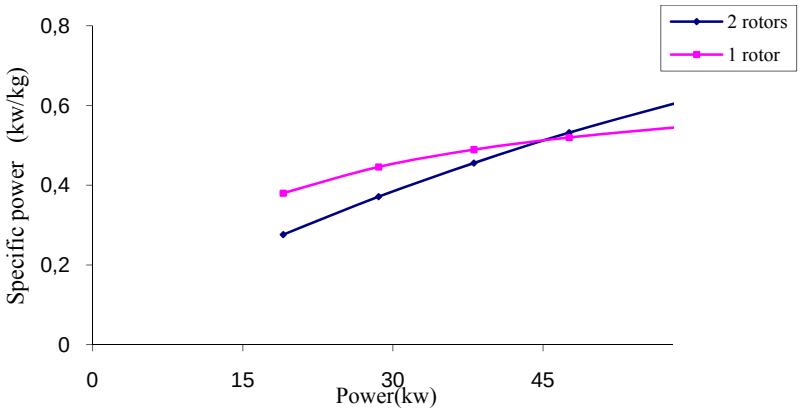

Figure 16: Specific power of a motor with one rotor and of a motor with double rotor

Figures 17 and 18 represent respectively the variation of the volume and power density of the motor versus to the power for the two structures, simple and double rotor motor.

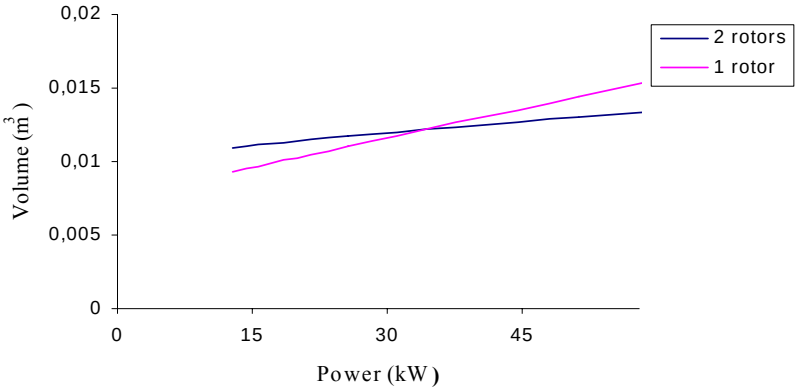

Figure 17: Motor volume of a motor with one rotor and of a motor with double rotor

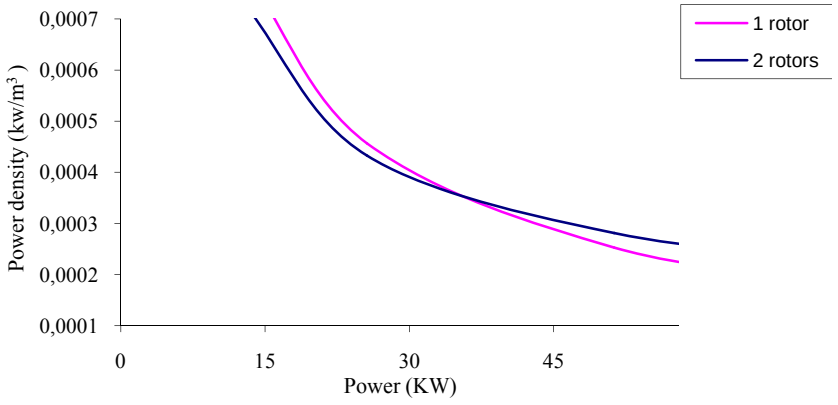

Figure 18: Motor power density of a motor with one rotor and of a motor with double rotor

We deduce that for a power superior to 40 kW, the volume of double rotor motor is lower than those of simple rotor motor.

6. MODELLING OF THE CONVERTER LOSSES

The objective of this part is to find out a converter losses model that can integrate in an energy optimization approach way algebraically. In a first phase, we present the model of the converter losses including the losses at conduction and the losses at commutation. In a second phase, we show that the losses of the converter in the majority depending on the load current.

6.1. DIAGRAM OF THE THREE-PHASE INVERTER

The motor is fed by a three-phase inverter, which is current reversible to assure the recuperation of the energy during the deceleration phases. The current control in the motor is assured by pulse width modulation.
The diagram of a three-phase inverter at two levels of tension consists of 6 commutations cells, IGBT and diodes.

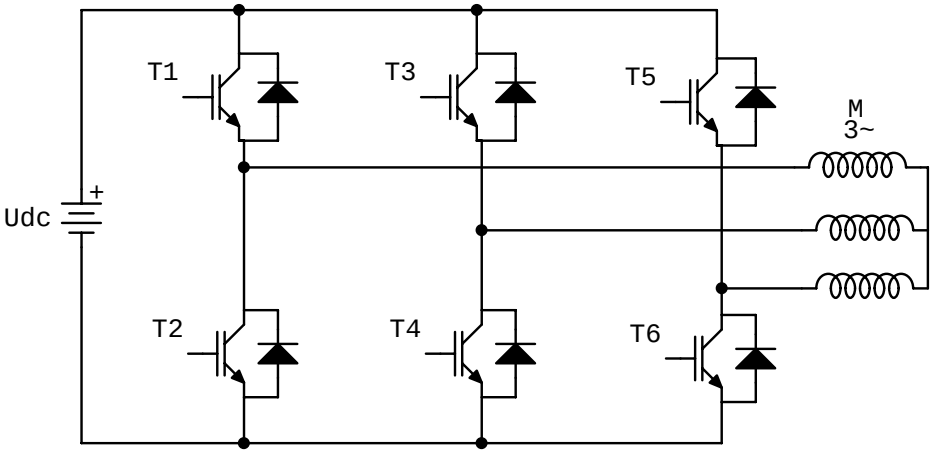

Figure 19: Diagram of the three-phase inverter

6.2. MODELLING OF THE CONVERTER LOSSES

In an electric energy converter operating at forced commutation, the losses may be divided into two parts:
– Conduction losses
– Commutation losses
The losses at conduction will be sensitive to components terminals voltage and to phase current, which go through it during a certain time, which is dependent on the cyclic ratio.
The losses at commutation depend on the dissipated energy at the transistors moment state changes. These losses are proportional to the splitting frequency of the converter.
The conduction losses of a converter arm deduced from this operation mode will be expressed through the following formula:

$$P_{cond} = 2\rho V_{ce}(I).I + (1-\rho)V_d(I).I \quad (60)$$

With I is the phase current, V_{ce} is the emitter-collector tension and V_d is the tension drop at the diode level [15], ρ being the cyclic ratio.
The collector emitter voltage and the diode level are given respectively:

$$\text{IGBT: } V_{ce} = f(I) = V_{ceK1} \ln\left(1 + \frac{I}{V_{ceK2}}\right) + V_{ceK3} I + V_{ceK4} I^2 \quad (61)$$

$$\text{Diode: } V_d = f(I) = V_{dK1} \ln\left(1 + \frac{I}{V_{dK2}}\right) + V_{dK3} I + V_{dK4} I^2 \quad (62)$$

$V_{cek1,}$ $V_{cek2,}$ V_{cek3} and V_{cek4} : are constants characterizing the transistor.
V_{dk1}, V_{dk2}, V_{dk3} and V_{dk4} : are constants characterizing the diode.
The losses by commutation of a converter arm deduced from this operation mode will to expressed through the following expression
IGBT:

$$P_{com} = \left(K_{Eon} E_{on}(I) + K_{Eoff} E_{off}(I)\right) f_{sw} \quad (63)$$

With f_{sw} is the commutation frequency.
K_{Eon} and K_{Eoff} are corrections factors, which are proportional to the direct voltage, applied to the converter

$$K_{Eon} = K_{Eoff} = \frac{U_{dc}}{E_w} \quad (64)$$

Udc is continuous voltage of the test and E_W is the direct voltage issued from constructive tests since the energy determination wasted at the closure and at the opening. [15]
E_{on} is the energy dissipated at the opening, its expression is given by:

$$E_{on}(I) = E_{onk1} \ln(1 + \frac{I}{E_{onk2}}) + E_{onk3} I + E_{onk4} I^2 \quad (65)$$

Where $E_{onk1,}$ $E_{onk2,}$ E_{onk3} and E_{onk4} are constants, which characterize the transistor at the opening.
The dissipated energy at the closure E_{off} is expressed as follows.

$$E_{off}(I) = E_{offk1} \ln(1 + \frac{I}{E_{offk2}}) + E_{offk3} I + E_{offk4} I^2 \quad (66)$$

Where $E_{offk1,}$ $E_{offk2,}$ E_{offk3} and E_{offk4} are constants that characterize the transistor at the closure.
The commutation losses at diodes are neglected.

6.3. MODEL OF CONVERTER LOSSES

For this approach, we deduce that the converter losses depend on the cyclic ratios, the current of each arm, of the direct tension and of the converter commutation frequency.

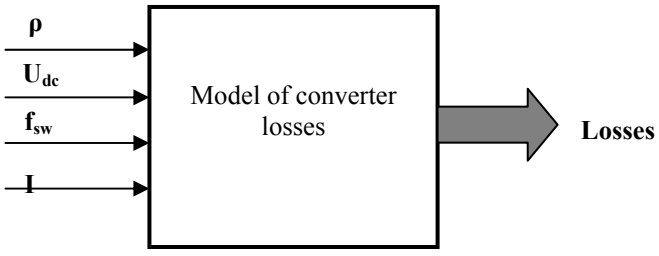

Figure 20: Model of converter losses

6.4. LOSSES VARIATION IN FUNCTION TO THE DIRECT VOLTAGE

The objective of this simulation is to study the converter losses in function to the direct voltage U_{dc}. The figure 21 shows the losses variation compared to U_{dc}.

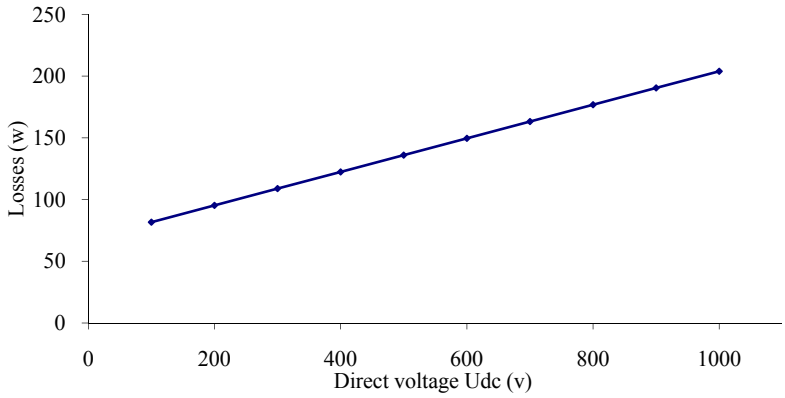

Figure 21: Variation losses in function to the direct tension U_{dc}

We note that converter losses depend slightly on the direct voltage. Indeed, the voltage variation influences the conduction losses of the diodes and transistors.

6.5. LOSSES VARIATION IN FUNCTION TO THE COMMUTATION FREQUENCY

In this configuration, we fix the direct voltage and the load current at constant values.
We carry out a simulation by varying the commutation frequency. The figure 22 shows the losses variation in function of f_{sw}.

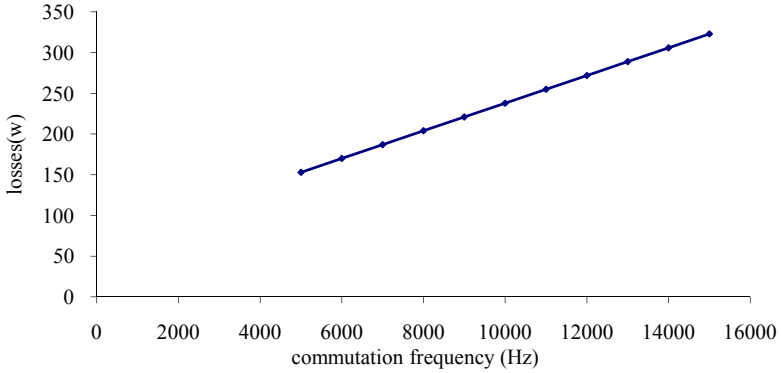

Figure 22: losses Variation in function to the commutation frequency f_{sw}

The commutation frequency is not an important parameter for the converter losses variation. The frequency variation influences the commutation losses.

6.6. LOSSES VARIATION IN FUNCTION TO THE LOAD CURRENT

To study the losses variation of the converter in function to the current I, we carry out a simulation by varying the load current. The figure 23 represents the variation of these converter losses in function to I.

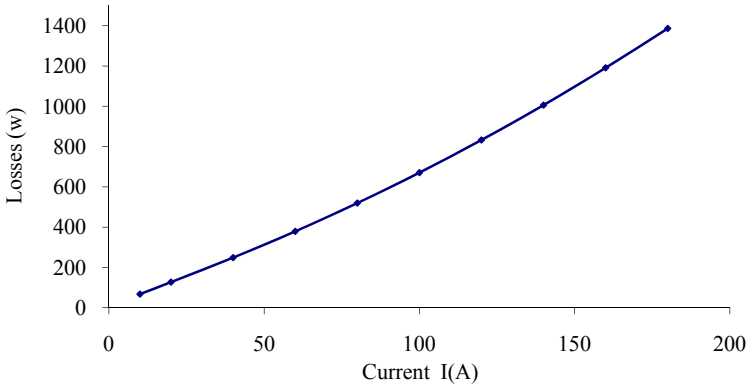

Figure 23: Converter losses in function to the current I

The losses in the converter depend on the current in the load; consequently, the converter losses can be represented by a second-order polynomial function depending on the load current. The polynomial coefficients of the losses model are functions of the direct voltage and of the commutation frequency.

7. Efficiency Optimization of the All Converter-Motor

The efficiency optimization consists in finding out same parameters of dimensioning chosen as variables input to maximize the efficiency at a nominal operation point.
The efficiency of the set converter-motor is defined as being the ratio of the output power by the input power, which is expressed as follows:

$$\eta = \frac{T_u \Omega}{T_u \Omega + P_J + P_f + P_m + P_{con} + P_{com}} \tag{67}$$

Where

- T_u : output torque
- P_j : copper losses
- P_m: mechanical losses
- P_f: stator core losses

The copper losses of the motor at the nominal operation point are expressed as follows:

$$P_j = 3\, R_{cu} \left[1 + \alpha \left(T_b - 20\right)\right] \left[\frac{N_{sph1}\, \delta\, L_{sp1}}{I_{ph}/\sqrt{2}} + \frac{N_{sph2}\, \delta\, L_{sp2}}{I_{ph}/\sqrt{2}} \right] {I_{ph}}^2 \tag{68}$$

The mechanical losses at the nominal operation point of the motor are expressed by:

$$P_m = K_m P_{em} \tag{69}$$

Where K_m is the mechanical losses coefficient.
The losses iron at the nominal operation point of the motor are given by [16]

$$P_f = q \left(\frac{f_b}{50}\right)^{1.5} \left[M_{cs1} B_{cs1}^2 + M_{ds1} B_{d1}^2\right] + q \left(\frac{f_b}{50}\right)^{1.5} \left[M_{cs2} B_{cs2}^2 + M_{ds2} B_{d2}^2\right] \tag{70}$$

Where:

- f_b: base feeding frequency of the motor
- q: loss value of the steel grade at 50 Hz and at the flux density of 1 T

The conduction and commutation losses of the converter are given by the following expressions:

$$P_{cond} = 2\rho V_{ce}(I).I + (1-\rho)V_d(I) \quad (71)$$

$$P_{com} = \left(K_{Eon}\, E_{on}(I) + K_{Eoff}\, E_{off}(I)\right) f_{sw} \quad (72)$$

The conception parameters (the current density δ in the slots, the magnetic inductions B_e in the air-gap, B_{cr} in the rotor yoke and B_{CS} in the stator yoke) of the motor, which maximize the efficiency of the set motor-converter can be optimized by an optimization method.

8. CONCLUSION

The study consists in designing of a double rotor motor for an electric vehicle. A stage of the dimensioning study was to define what are the variable or invariable input parameters and the output results. The task, then, consisted in linking the input parameters defined by the specification and by designer, by analytical equations.

A finite elements method is done dynamically so as to validate the assumptions made during analytical dimensioning and to validate wave forms that depend strongly on the machine geometry as well as the electromagnetic motor torque.

A comparison between the motor with double rotor and the motor with one rotor, gives many advantages. One of the advantages procured by two rotors, is to answer the torque characteristic, required at the starting.

The machine is controlled by an inverter, it is indispensable to take into account the converter losses. An average model of inverter is used to obtain a losses simplified model.

The model can be integrated in our optimization approach.

REFERENCES

[1] Qu, R., Aydin, M., Lipo, T.A.: Performance Comparison of Dual-Rotor Radial-Flux and Axial-Flux Permanent-Magnet BLDC Machines. In Proceedings of IEEE Electric Machines and Drives Conference, IEMDC'03, Madison, United States, 1-4 June 2003, Vol. 3, pp. 1948-1954.

[2] Tounsi S., Neji R., Gzara M. and Sellami F.: Cost Reduction of Permanent Magnet Synchronous Motor with Axial Flux. Accepted paper at ICEM-04 (16th International Conference on Electrical Machines), 5-8 September 2004, Cracow-Poland.

[3] Stephen W. Moore, Khwaja M. Rahman and Mehrdad Ehsani: Effect on Vehicle Performance of Extending the Constant Power Region of Electric Drive Motors, SAE TECHNICAL PAPER SERIES 1999-01-1152 International Congress and Exposition Detroit, Michigan March 1-4, 1999. Reprinted From: Advances in Electric Vehicle Technology (SP-1417).

[4] Iqbal H. and Mohammad S. I.: Design, Modelling and Simulation of an Electric Vehicle System. SAE TECHNICAL SERIES 1999-01-1149 International Congress and Exposition Detroit, Michigan March 1-4, 1999 Reprinted From: Advances in Electric Vehicle Technology (SP-1417).

[5] Sitapati K., Krishnan R.: Performance Comparisons of Radial and Axial Field Permanent-Magnet, Brushless Machines. IEEE Transactions on Industry Applications. Vol. 37, No. 5, 2001, pp. 1219-1226.

[6] Brisset S., Gillon F., Brochet P. : Manufacturing Cost Reduction in Brushless DC motors. ICEM2002, 26-28 August 2002, Bruges-Belgium, CD: ICEM02-546.

[7] Tounsi S., Gillon F., Brisset S., Brochet P., Neji R.: Design of an Axial Flux Brushless DC Motor for Electric Vehicle. ICEM2002, 26-28 August, Bruges-Belgium, CD: ICEM02-581.

[8] Salminen P.: Fractional Slot Permanent Magnet Synchronous Motors For Low Speed Applications. Dissertation. Lappeenranta University of Technology, Finland, 2004, p. 150.

[9] Sahin F.: Design and Development of a High-Speed Axial-Flux Permanent-Magnet Machine, Dissertation. Eindhoven University of Technology, The Netherlands, 2001, p. 228.

[10] Qu R., Lipo T.A.: Analysis and Modeling of Air-Gap and Zigzag Leakage Fluxes in a Surface-Mounted Permanent Magnet Machine. IEEE Transactions on Industry Applications. Vol. 40, No. 1, 2004, pp. 121-127.

[11] Parviainen A., Niemelä M., Pyrhönen, J.: A Novel Axial-flux Permanent Magnet Machine to Laboratory Use, In Proceedings of 11th International Symposium on Electromagnetic Fields in Electrical Engineering, Maribor, Slovenia, 18-20 September 2003, pp. 277-280.

[12] Parviainen A., Niemelä M., Pyrhönen J.: Modeling Axial-flux Permanent-Magnet Machines. IEEE Transaction on Industry Applications. Vol. 40, No. 5, 2004, pp. 1333-1340.

[13] MAXWELL®: Ansoft Corporation' Four Station Square-Suite 660 Pittsburgh PA 15219 USA .

[14] Huang S., Luo J., Leonardi F., Lipo T.A.: A Comparison of Power Density for Axialflux Machines Based on General Purpose Sizing Equations. IEEE Transactions on Energy Conversion. Vol. 14, No. 2, 1999, pp. 185-192.

[15] Bastiani P : Stratégies de Commande Minimisant les Pertes d'un Ensemble Convertisseur Machine Alternative : Application à la Traction Electrique. Thèse soutenue le 23 Février 2001, INSA de Lyon, France.

[16] Vogt K.: Elektrische Maschinen, VEB Verlag Technik, 1983, p. 500. Berlin-Germany.